Microscopic photoluminescence and photocurrent imaging spectroscopy of InAs nanostructures: Identification of photocarrier generation sites for intermediate-band solar cells

David M. Tex,[1,2] Toshiyuki Ihara,[1] Itaru Kamiya,[3] and Yoshihiko Kanemitsu[1,2,*]
[1]*Institute for Chemical Research, Kyoto University, Uji, Kyoto 611-0011, Japan*
[2]*Japan Science and Technology Agency, CREST, Uji, Kyoto 611-0011, Japan*
[3]*Toyota Technological Institute, Nagoya, Aichi 468-8511, Japan*
(Received 4 September 2013; revised manuscript received 25 February 2014; published 11 March 2014)

We performed microscopic imaging of photoluminescence (PL) and photocurrent (PC) on InAs nanostructures including disklike structures (nanodisks) and quantum dots (QDs). The correlation between PL and PC images indicates that the major fraction of upconverted carriers originates from nanodisks. By analyzing the excitation spectra, we find evidence that nanodisks and QDs need to be spatially separated to enhance PC generation via upconversion. The efficient simultaneous use of both QDs and nanodisks is an alternative approach to intermediate-band solar cells, where low-energy photons are upconverted in the QDs and high-energy photons are efficiently upconverted in the nanodisks, resulting in enhanced carrier generation yields. With spatially resolved upconverted PL, we show that PC generation in nanodisks is due to ejection of both electrons and holes.

DOI: 10.1103/PhysRevB.89.125301 PACS number(s): 84.60.Jt, 72.40.+w, 78.66.Fd, 73.50.Pz

I. INTRODUCTION

Since the seminal work by Shockley and Queisser (SQ) in 1961 [1], there has been an ongoing intense discussion on the physics of solar cells and how to raise solar cell efficiency. The SQ analysis determined for the first time the theoretical conversion efficiency limit of single junctions. Their concept has led to a depiction of possible improvements to other solar cells as well. To overcome the SQ limit of a single junction solar cell, multiple junctions [2] or novel carrier generation sites are required.

In particular, the new solar cell concepts based on nanostructures have attracted much attention, since nanostructures may realize high-energy conversion efficiencies that are not possible with bulk materials, through unique energy conversion processes, such as multiple exciton generation [3–7] or upconversion [8,9]. The former results in the formation of two or more excitons upon absorption of a single photon, enhancing the number of carriers that are generated. In contrast, upconversion is a process through which two or more low-energy photons are converted to one high-energy carrier. Upconversion can be applied for realizing intermediate-band (IB) solar cells [10], which reduce the losses that arise from low-energy photons not being absorbed by bulk material [11]. This is achieved by introducing an intermediate state in the semiconductor band gap. Following the absorption of sub-band-gap photons by the intermediate state, carriers are created in the conduction and valence bands of the bulk material by upconversion. Such an intermediate state can be readily designed with nanostructures, and the device properties are determined by the design. Therefore, optimizing the nanostructure design is crucial to realize high efficiencies.

InAs nanostructures have attracted special attention in the past decade as a model material for IB solar cells [11]. Two classes of InAs nanostructures are of particular importance: quantum dots (QDs) [12,13] and disklike structures [nanodisks, also referred to as quantum-well islands (QWIs)] [14], both of which can be prepared by self-assembly during epitaxial growth of InAs on (Al)GaAs. Using upconverted photoluminescence (PL), it has been verified that upconversion in shallow confined nanodisk states exhibits higher upconversion efficiencies than that in deep QD states [15–17]. Efficient photocurrent (PC) generation in nanodisks has also been observed and has been assigned to occur via Auger processes [18]. However, the IBs formed by InAs QDs have been the focus of research, because their deeply confined states provide broad spectral absorption [11]. High efficiencies for ideal IB solar cells have been predicted theoretically [10], but PC generation from the InAs QD layers grown with techniques such as molecular beam epitaxy (MBE) or metalorganic chemical vapor deposition (MOCVD) is still too small for application to solar cells [19–23]. The in-plane density and spatial distribution of the QDs can be varied by the growth conditions, and for densities smaller than about $10^{11}/\mathrm{cm}^2$, QDs and nanodisks usually coexist in the InAs layer. Spatial distribution of QDs and nanodisks affect PC generation, depending on the upconversion mechanisms. Upconversion in these structures has been studied previously by examining the temperature dependence of PC spectra. The major upconversion mechanisms are thermal activation for QDs [24] and Auger processes for nanodisks [18], and their PC generation efficiencies are strongly different. Using microscopic imaging spectroscopy [25], selective investigation in areas with small or large QD densities is possible, leading us to clarify the photocarrier generation sites and the energy transfer between nanodisks and QDs.

In this work, we performed a microscopic imaging of PL and PC on InAs nanostructures. We observed a strong correlation between the PL and PC of nanodisks, while no such correlation was observed in the QD region. This is attributed to efficient photocarrier generation in the nanodisks, via carrier upconversion of sub-band-gap photons. We show experimental evidence that QDs quench PC generation in nanodisks in certain areas of the InAs layer. Due to the imaging spectroscopy of PL and PC, we find that this quenching is due to the presence of an energy transfer from nanodisks to QDs. It is shown that in regions where QDs are separated from

*kanemitu@scl.kyoto-u.ac.jp

nanodisks, no quenching occurs. We conclude that InAs QDs and nanodisks need to be spatially separated to obtain high photocarrier generation efficiency. The upconverted PL and PC images show that the carrier upconversion in nanodisks occurs through simultaneous ejection of both electrons and holes, to the conduction and valence bands of the barrier material, respectively, through the Auger process in a nanodisk.

II. EXPERIMENT AND SAMPLE STRUCTURES

The sample used in this work was prepared by MBE on a semi-insulating GaAs (001) substrate, and it has been discussed in our previous report [18]. The conduction-band structure of the sample is illustrated in Fig. 1(a). After growing a GaAs buffer layer, an AlGaAs barrier (Al content ≈20%) containing an InAs layer and a GaAs/AlGaAs quantum well (QW) for measurement of upconverted PL were grown. On top of this structure, a GaAs layer containing a second thin InAs layer was prepared.

The amount of InAs buried in AlGaAs is 2.2 monolayers (MLs) and contains 2- and 3-ML-thick nanodisks as well as QDs. The InAs QDs formed through the Stranski-Krastanov (SK) growth mode, where nucleation of QDs occurs when the deposition thickness exceeds the so-called critical thickness, in the present case nominally 1.7 ML [12,13]. The QDs are usually a few nm in height and about 30 nm in diameter, whereas the nanodisks are only a few ML (preferentially 2 and 3 ML) in height and several times larger in diameter than the QDs. Since the thickness of the nanodisks is less than the height of the QDs, the quantum confinement along the growth direction is stronger in the nanodisks. Consequently, the quantized states of the InAs/AlGaAs nanodisks are at higher energies (shallow states, with total barrier height for the electron and hole of ≈230 meV) than those of the InAs/AlGaAs QDs (total barrier height >390 meV). In contrast, the amount of InAs buried in GaAs was intentionally set at 1.4 ML, below the critical thickness. This results in the formation of 2- and 3-ML-thick nanodisks only, i.e., no QDs are formed. The confined energies of InAs/GaAs nanodisks lie at an intermediate level, providing us with the opportunity to investigate the barrier height dependence on PC generation. Moreover, if the in-plane coupling between electronic states of the nanostructures is too large, carrier generation becomes a delocalized process. To avoid in-plane coupling, we start from single InAs layers with relatively low nanostructure densities. For relatively small QD in-plane densities, $<10^{11}/\mathrm{cm}^2$, the InAs layer usually contains considerable amounts of both QDs and nanodisks [18], while electronic coupling should only occur between very close next-neighbor nanostructures. As a result of the growth mechanism, regions with the highest QD densities are different from those with the highest nanodisk densities, and thus spatial separation of PC generation through QDs and nanodisks is possible in such low-density QD layers.

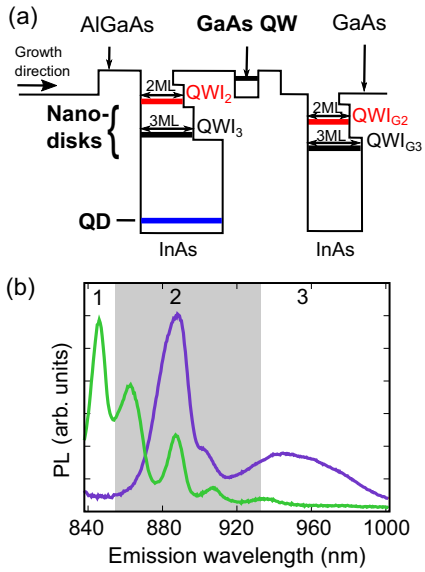

FIG. 1. (Color online) (a) Conduction-band diagram of sample structure. Growth proceeds from left to right. On top of a GaAs substrate, an InAs/AlGaAs layer with shallow 2 ML nanodisk states (QWI_2, red), 3 ML nanodisk states (QWI_3, black) and deep QD states (blue) was grown. Then a GaAs QW was inserted for upconverted PL measurements. The top consists of an InAs/GaAs layer with the intermediate 2 (QWI_{G2}) and 3 ML (QWI_{G3}) nanodisk states indicated in red and black, respectively. (b) Stokes μPL spectra at selected points for excitation at 835 nm. Regions 1 and 3 correspond to spectral regions containing QWI_2 and QD states, respectively. Region 2 is explained in the text. The peak assignments are summarized in Table I.

The PL spectra were recorded with a 30 cm monochromator in combination with a liquid-nitrogen-cooled InGaAs detector. For the PC measurements, we prepared an Au contact on top of the sample and an In contact on the backside. All measurements were performed in a cryostat with a sample temperature of ≈60 K at a bias voltage of 0.9 V. For such intermediate temperatures, the PC signals through Auger processes are enhanced compared to lower temperatures, while the PL signals are still strong enough even for short integration times. For the applied bias, the confined energy levels do not shift significantly with respect to zero bias. Our experimental setup allows us to measure PC and PL excitation (PLE) spectra simultaneously. Complementary information is obtained by PL and PC to understand the details of carrier dynamics [26], and this allowed us to determine the upconversion mechanism in the present nanostructures using macroscopic measurements [18]. By extending this technique to micro-PL (μPL) and micro-PC (μPC), the spatial distribution of generation and recombination sites in nanostructures can be revealed, which is important to determine different aspects of the nanostructures for solar cells. The μPL and μPC measurements were carried out over a spatial range of 60 μm × 60 μm with 2 μm step size with a 50× objective lens (NA = 0.42). For excitation, we used a continuous-wave tunable Ti:sapphire laser, at an intensity of ≈1 mW.

To obtain the spatially resolved Stokes PL image, we recorded one Stokes PL spectrum at each point of the 60 μm × 60 μm map. Two examples of such μPL spectra are shown in Fig. 1(b). Several states are resolved in the spectra; the high-energy peak at 845 nm [Fig. 1(b), region 1] and the broad low-energy peak at around 955 nm [Fig. 1(b), region 3] are assigned to the shallow 2 ML nanodisk (referred to in the following as the QWI_2 state) and deep QD states in AlGaAs,

TABLE I. Summary of peak assignments.

Structure	Barrier	Abbrev.	Peak pos. (nm)
2 ML nanodisk	AlGaAs	QWI_2	845–855
3 ML nanodisk	AlGaAs	QWI_3	875–890
Quantum dot	AlGaAs	QD	950–1150
2 ML nanodisk	GaAs	QWI_{G2}	860–870
3 ML nanodisk	GaAs	QWI_{G3}	900–915

respectively [18]. The peaks in region 2 are assigned to the intermediate nanodisk states: 3-ML-thick nanodisk states in AlGaAs (QWI_3 state, 875–890 nm), 2 ML nanodisks in GaAs (QWI_{G2}, 860–870 nm), and 3 ML nanodisks in GaAs (QWI_{G3}, 900–915 nm). The peak assignments are summarized in Table I. To clarify the mechanism that determines high and low efficiency PC generation sites, we mainly discuss the PL intensities of the shallow QWI_2 state and deep-lying QD state in connection to the PC signals. Discussion of the shallow QWI_2 can be done in a relatively clear manner, since 2 ML nanodisks are formed spatially separated from the QDs, while that of the intermediate QWI_3 state is complicated since 3-ML-thick nanodisks are formed closer to the QDs.

III. RESULTS

A. Spatial correlation of PL and upconverted PC from nanodisks

First, we discuss the PL and PC from 2 ML nanodisks in the InAs/AlGaAs layer (QWI_2). The μPL map for QWI_2 is shown in Fig. 2(a). The map is made by extracting the spectral PL intensity at each area of the 60 μm $\times$ 60 μm map for $\lambda_{PL} = 845 \pm 2$ nm [Fig. 1(b)] when excited at $\lambda_{ex} = 835$ nm. The areas with strong PL in Fig. 2(a) (for example, within the white broken border) show those with dense 2 ML nanodisks. The μPC map for direct excitation of the QWI_2 state with $\lambda_{ex} = 845$ nm is shown in Fig. 2(b). Because this excitation energy is smaller than the GaAs and AlGaAs barrier energies, the measured PC is due to upconversion of carriers from the InAs nanostructures. In the μPC map, we observe distributions similar to that in the corresponding μPL map in Fig. 2(a). For example, the areas showing strong PL, indicated with the white broken line, are strongly correlated with the areas showing strong PC. Whereas in macroscopic measurements the importance of shallow nanodisk structures was discussed using excitation spectra [18], the spatial correlation of the μPL and μPC maps more directly indicates that sites with many shallow nanodisks are essential for PC generation.

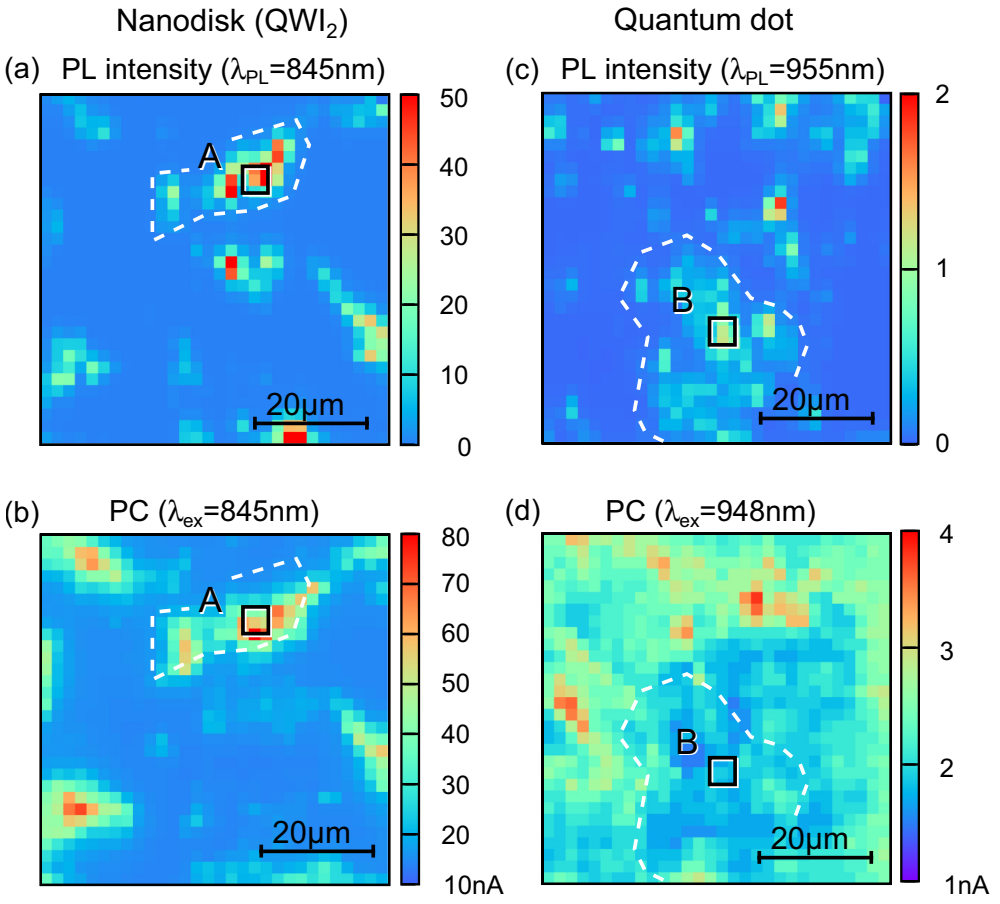

FIG. 2. (Color online) (a) μPL map of the $\lambda_{PL} = 845 \pm 2$ nm signal (2 ML nanodisks in AlGaAs, QWI_2) for excitation at $\lambda_{ex} = 835$ nm. (b) μPC map by exciting QWI_2 with $\lambda_{ex} = 845$ nm. Strong nanodisk PL is for the example observed in the areas within the white broken border. (c) μPL map of 955 ± 2 nm signal (QD) for excitation at $\lambda_{ex} = 835$ nm. (d) μPC map for excitation of QDs at $\lambda_{ex} = 948$ nm. The areas in the center, bordered by the white broken line, are those of strong QD PL. The scale bar for PL and PC is the same in both panel types.

B. Spatial correlation of PL and upconverted PC from QDs

Next, the PL and PC generation in QDs is investigated. The μPL map for the QD emission at $\lambda_{PL} = 955$ nm is shown in Fig. 2(c). The PL intensity scales in Figs. 2(a) and 2(c) are the same, so that the PL data can be compared directly. Overall smaller PL intensities are observed for the QD state than for QWI_2, because the image represents spectrally resolved data of the broad QD peak. The areas with strong QD PL (areas within the white broken line) are different from those where strong QWI_2 PL arise. This is a result of the spatial separation of areas with dense QDs and dense 2 ML nanodisks. Since QDs generally are formed upon epitaxial deposition of InAs on (Al)GaAs(001) over the critical thickness, this separation is realized under typical growth conditions inclusive of the present. Additionally, the μPC map for excitation of QDs with $\lambda_{ex} = 948$ nm is shown in Fig. 2(d): areas that show strong PL from QDs do not contribute effectively to PC generation. Rather, we found an anticorrelation between PL and PC images [areas within the white broken line in Figs. 2(c) and 2(d)].

C. Energy transfer between nanodisks and QDs

The spatial PL intensity distribution is primarily caused by the fluctuation in the nanodisk and QD distribution due to surface roughness and strain-driven growth mechanisms [12]. Such inhomogeneities result in potential fluctuations with deep valleys due to QD states, which bear possible recombination centers. Consequently, for interpretation of the PC measurements we need to consider energy transfer from the shallow (high-energy) nanodisk states to the deep (low-energy) QD states. With regard to the upconversion mechanism in Fig. 2(b), two possibilities are considered: (i) photoabsorption and upconversion of carriers in QWI_2, and (ii) photoabsorption in QWI_2 and upconversion of carriers from QDs via energy transfer between QWI_2 and QDs. Because a perfect coincidence of QWI_2 and QD distribution is highly unlikely in the SK growth, the observed strong correlation between PL and PC images indicates that energy transfer from QWI_2 to QDs is not involved in efficient PC generation through QWI_2.

Moreover, by comparing the QD μPL map [Fig. 2(c)] with the QWI_2 μPC map [Fig. 2(b)], it can be seen that the PC from QWI_2 is small in the areas with strong QD PL. The small PC of QWI_2 in areas with dense QDs (strong QD PL) can be explained with two models: (i) almost no 2 ML nanodisks exist in these areas, or (ii) optically excited 2 ML nanodisks lose their carriers to the energetically lower QDs by energy transfer. Since atomic force microscopy (AFM) measurements on uncapped samples in general do not show large nanodisk density fluctuations averaged over regions on the order of μm^2 [14], the anticorrelation of the QD PL and QWI_2 PC is likely due to an energy transfer process between the QWI_2 and QD state reducing the PC generation efficiency, and not due to an absence of QWI_2, which is also supported by excitation spectra shown below.

The μPL and μPC maps indicated that energy transfer between 2 ML nanodisks and QDs plays an essential role in efficient PC generation. Spectral information of the μPL and μPC maps also provide further insight into the mechanism of energy transfer involved in PC generation. To analyze

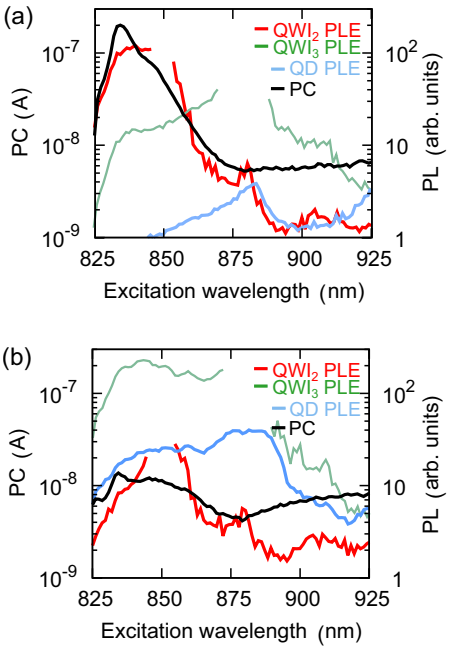

FIG. 3. (Color online) (a) μPC and μPLE spectra from area A indicated in Fig. 2. The PL detection wavelengths are $\lambda_{PL} = 845$, 880, and 955 nm, corresponding to the emission from 2 ML nanodisks in AlGaAs (QWI_2), 3 ML nanodisks in AlGaAs (QWI_3), and QDs, respectively. (b) PC and PLE spectra from area B, indicated in Fig. 2. The PL detection wavelengths are those of QWI_2, QWI_3, and QDs. The PLE spectra around the detection wavelengths are not shown. The scale bar is the same in both panels.

the mechanisms of PC generation in QWI_2, we compare the PC spectra of QWI_2 and QDs in area A, which shows both strong PC and PL as shown in Figs. 2(a) and 2(b). Figure 3(a) compares the PC spectrum (black) with the QWI_2 PLE spectrum (red), the QWI_3 PLE spectrum (green), and the QD PLE spectrum (blue), obtained at detection energies of $\lambda_{PL} = 845$, 880, and 955 nm, respectively. For excitation of QWI_2 [left half of Fig. 3(a), around 845 nm], we observe a strong PC signal as well as a strong QWI_2 PL signal. This suggests that the upconverted carriers are efficiently generated from QWI_2, in excellent agreement with macroscopic PC spectra [18]. At these excitation energies, the QD PL intensity is about 100 times smaller than that of QWI_2, and PL of QWI_3 is about ten times smaller. The large intensity ratio of PL from QWI_2 versus QD supports the idea that energy transfer from the shallow QWI_2 states to the deep QD states in area A is insignificant. Negligibly small energy transfer from nanodisks to QDs can be explained when the number of QDs located next to the nanodisks in this area is small. The existence of such spatial conformations is inferred from AFM images of uncapped samples [18]. In general, the energy transfer rate between two structures becomes weaker for larger distances. For resonant excitation of nanodisks, this means that QDs can become recombination centers when they are close to the 2 ML nanodisk structures [Fig. 2(b)]. This also leads to the following interpretation of PC under resonant QD excitation [Fig. 2(d)]. Because the QDs are sparse in regions outside B, the energy transfer to the deepest QD states (which are the preferential

recombination sites) is reduced, leading to slightly enhanced PC.

As for the PC generation in regions with QDs, the details of the energy transfer process can be deduced by comparing the excitation spectra of QWI_2 and QDs obtained from area B, which has a strong QD PL and a weak PC signal. As seen in Fig. 3(b), the QD PL intensity is stronger than the QWI_2 PL for all excitation wavelengths. This is in contrast to area A, where strong QWI_2 PL and weak QD PL were obtained. By comparing the PL intensities in Figs. 3(a) and 3(b), we find that in area B, for excitation at about 845 nm, the QWI_2 PL is weaker while the QD PL intensity is significantly stronger. Moreover, the PC in area B at this excitation is also decreased. The strong QWI_3 PL for excitation at $\lambda_{ex} = 845$ nm strongly suggests that 2 ML nanodisks actually exist in area B. The interchange of the PL intensities for excitation at about 845 nm can be explained when dense 3 ML nanodisks and QDs exist in the vicinity of the 2 ML nanodisks. In such a case, energy transfer from shallow 2 ML nanodisk states, where the carriers are generated, to deeper QD states occurs.

IV. DISCUSSION

A. Energy transfer model

The experimental results showed that PC is strong in regions with strong PL of QWI_2, whereas it is weak in regions with strong PL of QDs. The PL and PC excitation spectra verified that an energy transfer from QWI_2 to QDs reduces the PC generation in QWI_2. The most likely energy transfer process is a carrier transfer. After the carriers are transferred to the QDs, carrier recombination occurs preferentially due to low upconversion efficiency of carriers in QDs. This results in the weak PC signal from QDs. In the case of carrier transfer, the limiting factor for the PC generation efficiency is the electronic coupling. In the present case, we believe that this is determined by the tunneling from 2 ML nanodisks to QDs, directly or by using intermediate states such as 3 ML nanodisks. This model is supported by the enhanced QD PL signals for $\lambda_{ex} = 845$ and 890 nm from area B [Fig. 3(b)], corresponding to QWI_2 and QWI_3 states, respectively.

The PL and PC excitation spectra in Fig. 3(b) showed the importance of energy transfer between nanodisks and QDs. The spectroscopic investigation has revealed that a region where QDs and nanodisks coexist is not optimal for the overall PC generation because the carrier generation in the nanodisks is reduced due to energy transfer to QDs. To suppress such quenching of the carrier upconversion in nanodisks, it is important to isolate the nanodisks from the QDs.

The energy transfer model described in the previous paragraphs explains the experimentally observed reduction of PC from QWI_2 by an energy transfer from QWI_2 to QDs. In the following, we provide additional information to show that this model is consistent. First, PL and PC from QWI_3 are discussed, and then we show evidence that excitation of QDs through higher excited states is not dominant.

PL and PC images of QWI_3 are shown in Figs. 4(a) and 4(b), obtained from the same area for Fig. 2. Overall, the 3 ML nanodisks are formed close to the QDs, which is a feature of SK growth. In the right lower regions of Figs. 4(a) and 4(b), dense 3 ML nanodisks are observed, and in this region QDs are sparse. The improved PC contribution from the QWI_3 is attributed to less energy transfer to QDs. The enhancement of PC supports previous data [18], indicating that the upconversion mechanism of QWI_3 is similar to that of QWI_2, but less efficient than for QWI_2, which is probably due to the intermediate energy level not being optimal for carrier ejection, or being too close to that of the QDs. The PC image for $\lambda_{ex} = 880$ nm shows a PC peak distribution very similar to that obtained from QWI_2. The slightly enhanced PC of QWI_3 in the QWI_2 dominating area (for example, area A in Fig. 2) is observed because QDs are sparse and the carriers can be effectively excited.

The QD PL for near-resonant excitation at $\lambda_{ex} = 948$ nm is shown in Fig. 4(c). We observe all the bright PL regions which were also observed for nonresonant excitation at $\lambda_{ex} = 835$ nm in Fig. 2(c), and additional bright spots. Because the additional spots seen here were not observed for excitation with $\lambda_{ex} = 835$ nm, direct excitation of QDs through higher excited states can be discarded; the energy transfer from nanodisks is the dominant excitation mechanism under nonresonant conditions. Supporting evidence is obtained from PLE spectra of QDs. Because the PLE spectra for detection at $\lambda_{PL} = 955$ nm and also much longer wavelengths (>985 nm) are qualitatively the same, a resonant transfer from a nanodisk state to an excited QD state can be excluded.

So far we have discussed the features that are attributed to the InAs/AlGaAs layer. By using PC and PL spectra, we also identified the contributions from the InAs/GaAs layer. In the following, we show that the contributions from the nanodisks in the GaAs layer (QWI_{G2} and QWI_{G3}) are negligible.

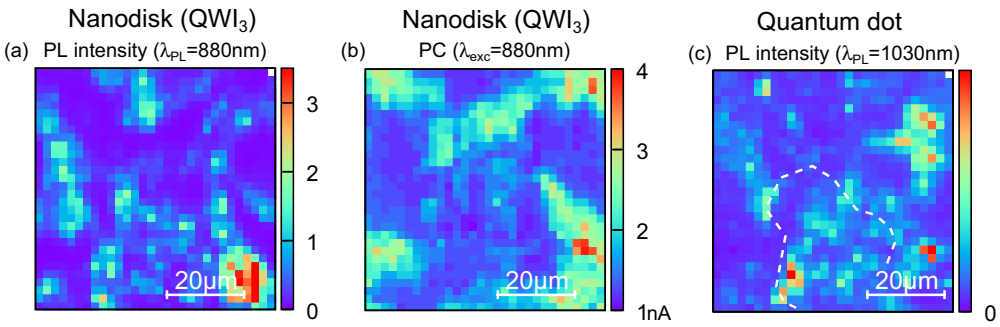

FIG. 4. (Color online) (a) PL of 3 ML nanodisks in AlGaAs (QWI_3) for $\lambda_{ex} = 835$ nm. (b) PC for $\lambda_{ex} = 880$ nm excitation. (c) QD PL for near-resonant excitation at $\lambda_{ex} = 948$ nm.

PL from QWI_{G2}, for example, is observed in Fig. 2(a), just below the area indicated with the white broken line (near the center of the image). The corresponding PC observed in Fig. 2(b) is several times weaker than that of QWI_2. We also note that small QWI_{G3} signals arise in the QD PC image in Fig. 2(d). Small PC contributions can be observed, for example, on the left side in Fig. 2(d). PC is visible there because the tail of QWI_{G3} extends down to about 948 nm, which is the excitation energy for this data set.

Positions of PC arising from the nanostructures in the InAs/GaAs layer have been verified to be different from the areas A and B indicated in Fig. 2. This suggests different quantum structure distributions in the two InAs layers, due to the stochastic processes involved in SK growth. The PC from the InAs/GaAs nanodisks is smaller than that for QWI_2, and thus they can at most provide the minority carriers for upconverted PL (recombination of carriers that were ejected from the InAs layers, discussed in the next section). Therefore, it is highly unlikely that simultaneous ejection of electrons from the InAs/AlGaAs layer and holes from the InAs/GaAs layer results in upconverted PL with exactly the same distribution as the QWI_2 PC shown in Fig. 2(b). Artifacts of the structures in the InAs/GaAs layer do not change our conclusions.

From the above discussion, we conclude that an energy transfer from nanodisks to QDs reduces the PC of nanodisks, and suppression of this process determines the efficient photocarrier generation sites.

B. Upconversion mechanism in nanodisks

The PC spectra indicated that the carrier generation efficiency of the QD is smaller than that of QWI_2. This is because the carrier upconversion mechanism is different for QWI_2 and the QD. The change of the carrier upconversion mechanism is a result of the different barrier heights [18]. Three upconversion mechanisms have been considered to date: thermal upconversion, two-step two-photon-absorption (TS-TPA) [8], and multicarrier Auger processes [9]. In the case of QDs, where upconversion from the deep states requires ejection of carriers over a large barrier, only thermal and TS-TPA processes are possible [24,27]. For nanodisks, the barrier height is much smaller, and thus multicarrier Auger processes can take place efficiently. The upconversion via Auger may be further enhanced by the large in-plane extension of the nanodisk structure, increasing two *e*-*h* pair formation. In our previous work [18], we determined that the upconversion mechanism in nanodisks is dominantly Auger with three experiments: (a) the temperature dependence data matching the Auger temperature dependence for activation energy of a few meV (i.e., the PC is almost constant for temperatures above about 100 K), much smaller than the barrier height; (b) the PC and PLE spectra, showing a very quick decrease of the upconversion efficiency for energies below that of QWI_3; and (c) the power dependence of PC and PL for excitation of QWI_2, showing a nearly quadratic behavior for low excitation power densities. We proposed that the Auger process in the nanodisks ejects both electrons and holes simultaneously, because this model is most plausible for the observed PLE spectra [15–17]. However, no direct evidence against an ejection of electrons and holes separately from different nanodisks could be provided with macroscopic measurements. The present microscopic study allows us to identify the energy transfer mechanisms as well as the origin of carriers required for PC and PL.

To obtain concrete evidence for the electron and hole ejection from QWI_2, we studied the spatial distribution of upconverted PL due to radiative recombination of electrons and holes in the GaAs/AlGaAs QW. For radiative recombination from the high-energy GaAs/AlGaAs QW, both electrons and holes in the conduction and valence band of the barrier, respectively, must be captured by the QW. To generate these carriers, simultaneous ejection of electron and hole from the nanodisks over the barrier is required. Upconverted PL is therefore additional evidence that tunneling is not dominantly responsible for PC. In Fig. 5, we compare (a) the PC from QWI_2 with (b) the upconverted PL from the GaAs/AlGaAs QW at $\lambda_{PL} = 740$ nm due to carriers created by upconversion in QWI_2 with excitation at $\lambda_{ex} = 835$ nm. A strong correlation of PC and upconverted PL is observed. The small background level is attributed to the diffusion of the electrons and holes, which is required to recombine in the QW, leading to a more diffusive image. This is supported by the PL image for excitation at $\lambda_{ex} = 880$ nm, which does not show any

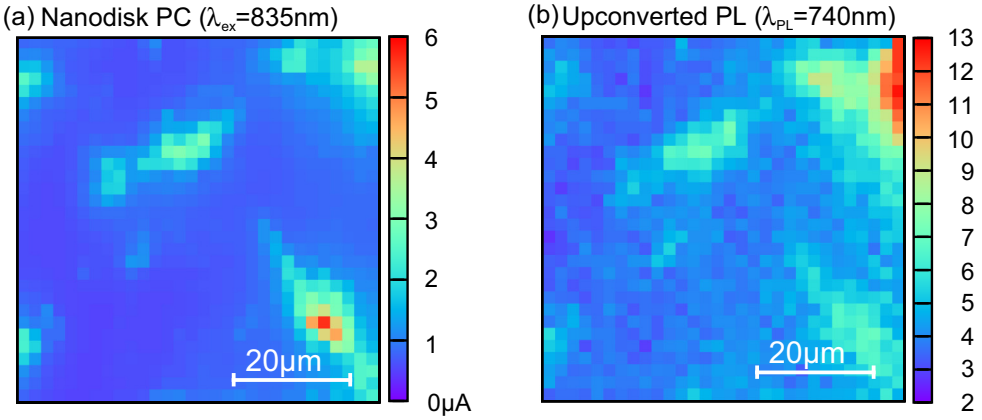

FIG. 5. (Color online) (a) PC map (excitation at $\lambda_{ex} = 835$ nm) and (b) upconverted PL map (excitation at $\lambda_{ex} = 835$ nm, detection at the GaAs QW state $\lambda_{PL} = 740$ nm). The sample temperature was ≈15 K.

background signal, thus discarding the possibility of deep trap states in the barrier being the origin.

The observed strong upconverted PL may be due to (i) electron and hole ejection from QWI_2, or (ii) electrons from QWI_2 and holes from the InAs/GaAs layer (QWI_{G2} or QWI_{G3}). In both cases, we conclude that QWI_2 ejects both the electron and the hole. Explanation (i) is trivial due to the very good agreement between upconverted PL and PC distribution. As discussed in Sec. IV A, (ii) is unlikely due to different distributions of nanodisk structures in both layers, but we shall consider it for completeness. In (ii) we consider that the holes from InAs/GaAs constitute the minority carriers, which are not observed in the PC images. To explain the temperature dependence in Ref. [18], QWI_2 must also eject holes. This is because a dominant electron current would require the electrons to overcome the AlGaAs barrier in the circuit, resulting in a strong temperature dependence (as verified for the GaAs PC in Ref. [15], but not for the InAs PC).

Therefore, the data verify that in the upconversion process in QWI_2, both electrons and holes are efficiently ejected to the barrier layers. This is either Auger ejection of a deeply confined hole with an additional thermal excitation of the electron, or dominantly Auger ionization of both carriers, without any thermal assistance. Considering the temperature dependence of upconversion via 2 ML nanodisks [15,18], ejection of both carriers via one or sequential Auger processes seems to be most plausible. The strong two-electron–hole pair interaction in QWI_2 is the reason why the PC generation efficiency of QWI_2 can exceed that of the QDs, and we verified that both types of carriers are ejected efficiently from QWI_2.

C. Application to solar cells

As discussed, an InAs layer usually consists of different quantum structures with different energy levels. The fact that upconversion in nanodisks and QDs occurs through different upconversion mechanisms and efficiencies needs to be taken into account to improve the efficiency of the InAs nanostructure-based IB solar cells. This is to say, the high-energy part of the solar spectrum should be upconverted via efficient shallow nanodisks, while the low-energy part of the solar spectrum should be upconverted with the deep-lying QDs. In a solar cell with only nanodisks, the narrow absorption spectrum will ultimately limit the ideal conversion efficiency (in the present case about 36%) [18]. By incorporating other structures with lower energy states such as QDs, broadband upconversion is possible and a significant additional PC generation is expected even in the case of low QD upconversion efficiency. However, multiple energy levels in a single layer imply additional possible relaxation paths. We verified this for QDs; when the QDs are close to the 2 ML nanodisks, both structures can couple, leading to quenching of the PC from QWI_2. By imaging spectroscopy of PC and PL, we verified the necessary application scheme which allows QDs to be used in parallel to nanodisks, without significant quenching effects. To suppress energy transfer in the form of carrier relaxation from nanodisks to QDs, they must be electronically decoupled, for example by being spatially separated from each other. This scheme provides an alternative IB solar cell concept, where the advantages of several nanostructures can be used. We note that the role of QWI_3 as a quenching site for QWI_2 is not necessarily the same as that of the QD, since the upconversion mechanism is different. The growth and control of structures where nanodisks and QDs are electronically decoupled will be a new challenge.

V. CONCLUSIONS

In summary, μPL and μPC measurements at low temperatures were employed successfully to provide information about PC generation in InAs nanostructures, where nanodisks and QDs coexist. PC generation for excitation of QDs is relatively small, while that for excitation of QWI_2 can be much stronger. The spatial resolved μPC map affirmed the conclusion that QWI_2 states are efficient PC generation sites. With the microscopy technique, we identified that the upconversion of carriers from QWI_2 causes the ejection of both electrons and holes, which are important for high PC generation efficiencies. It was shown that the energy transfer from QWI_2 to deep QD states is likely to occur when many QDs and nanodisks are located close to each other, quenching the upconversion from QWI_2. Imaging spectroscopy showed that for realizing highly efficient and broadband upconverting IBs, the arrangement of nanostructures with different upconversion mechanisms and efficiencies is a critical issue. We demonstrated that highly efficient shallow states should not be electronically coupled with low efficiency deep states, since energy transfer reduces the total conversion efficiency. Spatial separation of states with different upconversion efficiencies provides a method for designing more efficient IB solar cells through use of the most appropriate upconversion sites for each spectral component.

ACKNOWLEDGMENTS

Part of this work was supported by JST-CREST, KAKENHI (No. 25234567 and No. 25247052), and the Strategic Research Infrastructure Project, MEXT, Japan.

[1] W. Shockley and H. J. Queisser, J. Appl. Phys. **32**, 510 (1961).
[2] C. H. Henry, J. Appl. Phys. **51**, 4494 (1980); A. D. Vos, J. Phys. D **13**, 839 (1980); L. Zhu, C. Kim, M. Yoshita, S. Chen, S. Sato, T. Mochizuki, H. Akiyama, and Y. Kanemitsu, Appl. Phys. Lett. **104**, 031118 (2014).
[3] J. H. Werner, S. Kolodinski, and H. J. Queisser, Phys. Rev. Lett. **72**, 3851 (1994).
[4] A. J. Nozik, Physica E **14**, 115 (2002).
[5] R. D. Schaller and V. I. Klimov, Phys. Rev. Lett. **92**, 186601 (2004).
[6] A. Ueda, K. Matsuda, T. Tayagaki, and Y. Kanemitsu, Appl. Phys. Lett. **92**, 233105 (2008).
[7] O. E. Semonin, J. M. Luther, S. Choi, H.-Y. Chen, J. Gao, A. J. Nozik, and M. C. Beard, Science **334**, 1530 (2011).

[8] R. Hellmann, A. Euteneuer, S. G. Hense, J. Feldmann, P. Thomas, E. O. Göbel, D. R. Yakovlev, A. Waag, and G. Landwehr, Phys. Rev. B **51**, 18053 (1995).
[9] W. Seidel, A. Titkov, J. P. Andre, P. Voisin, and M. Voos, Phys. Rev. Lett. **73**, 2356 (1994).
[10] A. Luque and A. Marti, Phys. Rev. Lett. **78**, 5014 (1997).
[11] A. Luque, A. Marti, and C. Stanley, Nat. Photon. **6**, 146 (2012), and references therein.
[12] D. Leonard, M. Krishnamurthy, C. M. Reaves, S. P. Denbaars, and P. M. Petroff, Appl. Phys. Lett. **63**, 3203 (1993).
[13] V. Bressler-Hill, A. Lorke, S. Varma, P. M. Petroff, K. Pond, and W. H. Weinberg, Phys. Rev. B **50**, 8479 (1994).
[14] R. Heitz, T. R. Ramachandran, A. Kalburge, Q. Xie, I. Mukhametzhanov, P. Chen, and A. Madhukar, Phys. Rev. Lett. **78**, 4071 (1997).
[15] D. M. Tex and I. Kamiya, Phys. Rev. B **83**, 081309(R) (2011).
[16] C. Kammerer, G. Cassabois, C. Voisin, C. Delalande, Ph. Roussignol, and J. M. Gérard, Phys. Rev. Lett. **87**, 207401 (2001).
[17] P. P. Paskov, P. O. Holtz, B. Monemar, J. M. Garcia, W. V. Schoenfeld, and P. M. Petroff, Appl. Phys. Lett. **77**, 812 (2000).
[18] D. M. Tex, I. Kamiya, and Y. Kanemitsu, Phys. Rev. B **87**, 245305 (2013).
[19] A. Marti, E. Antoliin, C. R. Stanley, C. D. Farmer, N. Lopez, P. Diaz, E. Canovas, P. G. Linares, and A. Luque, Phys. Rev. Lett. **97**, 247701 (2006).
[20] A. Luque, A. Martin, N. Lopez, E. Antolin, E. Canovas, C. Stanley, C. Farmer, L. J. Caballero, L. Cuadra, and J. L. Balenzategui, Appl. Phys. Lett. **87**, 083505 (2005).
[21] W. Ye, S. Hanson, M. Reason, X. Weng, and R. S. Goldman, J. Vac. Sci. Technol. B **23**, 1736 (2005).
[22] D. Guimard, R. Morihara, D. Bordel, K. Tanabe, Y. Wakayama, M. Nishioka, and Y. Arakawa, Appl. Phys. Lett. **96**, 203507 (2010).
[23] Y. Okada, T. Morioka, K. Yosida, R. Oshima, Y. Shoji, T. Inoue, and T. Kita, J. Appl. Phys. **109**, 024301 (2011).
[24] E. Antolin, A. Marti, C. D. Farmer, P. G. Linares, E. Hernandez, A. M. Sanchez, T. Ben, S. I. Molina, C. R. Stanley, and A. Luque, J. Appl. Phys. **108**, 064513 (2010).
[25] S. Higuchi, A. Ishizumi, J. Sawahata, K. Akimoto, and Y. Kanemitsu, Phys. Rev. B **81**, 035207 (2010).
[26] Y. Yamada and Y. Kanemitsu, Appl. Phys. Lett. **101**, 133907 (2012).
[27] D. M. Tex, I. Kamiya, and Y. Kanemitsu, Sci. Rep. **4**, 4125 (2014).